Title
Major translocation of calcium upon epidermal barrier insult: imaging and quantification via FLIM/Fourier vector analysis

Journal
Archives of Dermatological Research, 303(2)

ISSN
0340-3696

Authors
Behne, Martin J
Sanchez, Susana
Barry, Nicholas P
et al.

Publication Date
2011-03-01

DOI
10.1007/s00403-010-1113-9

Arch Dermatol Res (2011) 303:103–115
DOI 10.1007/s00403-010-1113-9

ORIGINAL PAPER

Major translocation of calcium upon epidermal barrier insult: imaging and quantification via FLIM/Fourier vector analysis

Martin J. Behne · Susana Sanchez · Nicholas P. Barry · Nina Kirschner · Wilfried Meyer · Theodora M. Mauro · Ingrid Moll · Enrico Gratton

Received: 15 July 2010 / Revised: 6 December 2010 / Accepted: 7 December 2010 / Published online: 31 December 2010

Abstract Calcium controls an array of key events in keratinocytes and epidermis: localized changes in Ca^{2+} concentrations and their regulation are therefore especially important to assess when observing epidermal barrier homeostasis and repair, neonatal barrier establishment, in differentiation, signaling, cell adhesion, and in various pathological states. Yet, tissue- and cellular Ca^{2+} concentrations in physiologic and diseased states are only partially known, and difficult to measure. Prior observations on the Ca^{2+} distribution in skin were based on Ca^{2+} precipitation followed by electron microscopy, or proton-induced X-ray emission. Neither cellular and/or subcellular localization could be determined through these approaches. In cells in vitro, fluorescent dyes have been used extensively for ratiometric measurements of static and dynamic Ca^{2+} concentrations, also assessing organelle Ca^{2+} concentrations. For lack of better methods, these findings together build the basis for the current view of the role of Ca^{2+} in epidermis, their limitations notwithstanding. Here we report a method using Calcium Green 5N as the calcium sensor and the phasor-plot approach to separate raw lifetime components. Thus, fluorescence lifetime imaging (FLIM) enables us to quantitatively assess and visualize dynamic changes of Ca^{2+} at light-microscopic resolution in ex vivo biopsies of unfixed epidermis, in close to in vivo conditions. Comparing undisturbed epidermis with epidermis following a barrier insult revealed major shifts, and more importantly, a mobilization of high amounts of Ca^{2+} shortly following barrier disruption, from intracellular stores. These results partially contradict the conventional view, where barrier insults abrogate a Ca^{2+} gradient towards the stratum granulosum. Ca^{2+} FLIM overcomes prior limitations in the observation of epidermal Ca^{2+} dynamics, and will allow further insights into basic epidermal physiology.

Keywords Calcium · Lifetime imaging · Epidermis · Calcium Green 5N · DMSO · Phasor analysis

M. J. Behne (✉) · N. Kirschner · I. Moll
Department of Dermatology and Venerology,
University Medical Center Hamburg-Eppendorf,
Martinistr. 52, 20246 Hamburg, Germany
e-mail: m.behne@uke.uni-hamburg.de

S. Sanchez · E. Gratton
Laboratory for Fluorescence Dynamics,
Department of Biomedical Engineering,
University of California, Irvine, USA

N. P. Barry
Department of Nephrology,
University of Colorado Health Science Center,
Denver, CO, USA

W. Meyer
Anatomical Institute, University Veterinary Medicine Foundation,
Bischofsholer Damm 15, 30173 Hannover, Germany

T. M. Mauro
Veterans Affairs Medical Center Dermatology Departments,
University of California San Francisco, San Francisco, CA, USA

Introduction

Calcium is the ubiquitous second messenger system in cell biology (e.g., [17, 56]). In epidermis, it controls key events in epidermal barrier homeostasis and repair [48], neonatal barrier establishment [21], keratinocyte differentiation [32, 65], and signaling [73, 74], cell adhesion [2], and a range of pathologic states [49, 53]. Yet, tissue- and cellular-Ca^{2+} concentrations in physiologic and diseased conditions are only partially known.

To date, there are three well-established methods for calcium measurements in skin. Firstly, state of the art for complex tissues is calcium-PIXE (proton-induced X-ray emission). The publications employing this method have largely defined the current knowledge about the epidermal calcium gradient [9, 21, 46]. Nevertheless, this method measures total calcium concentrations over depth in a line-scan, irrespective of ionization-state or binding, and without information about cellular/subcellular (co-) localization. The resulting finding of a calcium gradient is therefore, in part, a mathematical artifact, i.e., the gradient might result less steep if the denominator were cellular layers, not tissue-depth. Further, calcium-PIXE requires tissue processing (sectioning followed by freeze drying), is only available in very specialized institutions, and is therefore limited to addressing only selected questions. Second, the other method that has been used frequently, a histochemical calcium-precipitation followed by transmission electron microscopy (TEM), requires extensive tissue fixation and processing, and is similarly not suitable for a close to in vivo assessment [49, 50, 78]. Third, calcium is measured in vitro using an array of fluorescent dyes (see below), or through transfection of targeted constructs (e.g., Aequorin) into cultured cells, measuring fluorescence or luminescence to quantify calcium in subcellular compartments [8, 63], creating detailed knowledge of intracellular calcium ranges and leading to insight on their roles [7].

The combined view from these reports renders a rough "map" of calcium values reported and to be expected in skin (please refer to Table 1). From cell culture experiments, where regulation of proliferation and differentiation through calcium levels is standard procedure (e.g., [7, 28, 42]), intracellular concentration ranges are established. Virtually, all organelles are Ca^{2+} stores [51], and in general, low cytoplasmic values (0.1 μM) are distinct from several fold higher organelle values (e.g., ER 500 μM) [17]. Reports about Ca^{2+} concentrations in skin are somewhat divergent, hardly comparable qualitative [48, 49] and quantitative methods [25], with the generally accepted values from PIXE experiments [47], where calcium from serum-like levels in the SB roughly triple in the SG, to abruptly drop below serum levels in the SC.

Together, these findings have defined the current view of calcium's role in skin, while observation in vivo/in situ is still lacking. The need for a method to measure and localize Ca^{2+} in tissue is therefore evident. Recent reviews on the topic point to an apparent lack of experimental options [8, 63], although lifetime imaging was not considered.

Fluorescence imaging and measurement of Ca^{2+} concentrations have been reported in numerous papers, using a variety of indicator dyes in different modalities, mostly to assess intracellular concentrations of many different cell types [14, 23, 83], as well as keratinocytes and their organelles (e.g., [4]). Also, advantages and disadvantages comparing Ca^{2+}-sensitive dyes and various methodologies for their use have been discussed extensively [35, 40, 41]. The general method of two-photon Ca^{2+} imaging has been described for various dyes [37]. Also, fluorescence lifetime imaging (FLIM) to determine Ca^{2+} concentrations has been tested before [1, 36, 69, 85], and is further detailed conceptually [16]. The first description for Calcium Green 5N (CaG5N) [59] discussed the advantages of its low Ca^{2+} affinity, avoiding the underestimations seen with other dyes [68], and thus indicating its usefulness for investigation in skin. In a parallel paper [11] we describe the heterogeneity of calcium distribution in human skin using FLIM, and a follow-up details the intracellular calcium-release following barrier perturbation at the SG–SC interface through pharmacologic manipulation [10].

This report is the continuation of our prior work where we successfully established FLIM to assess epidermal pH

Table 1 Table of reported/expected Ca^{2+} concentrations in skin

	Concentration ranges reported	References
SC	Low (comparable to SB); medium in lower SC, zero in outer SC; (very high)	[47], [49], [24, 25]
SB–SG	Gradient rising towards SG; low values for proliferating (SB), and high values for differentiating cells (SS and SG)	[24, 25, 47–49], [7, 28, 42]
Organelle	High	[17]
Dermis	Low, comparable to SG; serum levels	[47, 49], [71, 84]

The combined view of various reports renders a rough "map" of calcium values reported and to be expected in skin, with divergent findings in parentheses

In cell-culture experiments, regulation of keratinocyte proliferation and differentiation through calcium levels is standard procedure, and the concentration ranges are established for various mouse- and human-keratinocyte cell types and lines (e.g., [7, 28, 42])

Virtually, all organelles are Ca^{2+} stores [51], and in general, low cytoplasmic values (0.1 uM) are distinct from several fold higher organelle values (e.g., ER 500 uM) [17]

We exemplarily measured serum values for calcium (2.6 mmol/l), and inorganic phosphorous (3.3 mmol/l) in a male hairless mouse. These values are well in accordance with averages of 40 mouse strains displayed in The Mouse Phenome Database (http://aretha.jax.org/pub-cgi/phenome/mpdcgi?rtn=docs/home) [71]

Reports about Ca^{2+} concentrations in skin are somewhat divergent, hardly comparable qualitative [48, 49] and quantitative methods [25], with the generally accepted values from PIXE experiments [47], where calcium from serum-like levels in the SB roughly triple in the SG, to abruptly drop below serum levels in the SC

Although for skin a vacuum PIXE technique was applied [9], the values obtained there for dermis were quite similar to newer "air" measurement values for serum samples [31], which again compared well to standard serum electrolyte analyses [84], and their established reference values

[5, 26], demonstrating that this method overcomes the specific limitations of fluorescence-based measurements in complex tissues. Here, we tested this novel approach on the known inducible perturbation of Ca^{2+} homeostasis, epidermal permeability barrier abrogation in rodent skin. We found a fast, highly dynamic response to an experimental barrier insult, where details partially contradict the view established through earlier methods.

Methods

Materials

Calcium Green 1, Calcium Green 5N, Rhod 5N and calcium-calibration buffer kits were purchased from Molecular Probes (Eugene, OR). Calcium Chloride dihydrate (C3306, molecular biology grade), and BSA (Bovine Serum Albumin, A7030) were from Sigma-Aldrich, Germany.

Animal experiments

Male hairless mice (SKH1 h/hr, Charles River Laboratories, Wilmington, MA, USA) were fed Purina mouse diet and water ad libitum. Animals were 8–12 weeks old at time of experiments. Conventional surface pH measurements were performed using a flat glass surface electrode (Mettler-Toledo, Giessen, Germany) attached to a pH meter. The Stratum corneum (SC) was removed/stripped by several sequential strippings with D-squame disks (Academ, Menlo Park, CA, USA), inducing an increase in transepidermal water loss levels (TEWL) above base line (from ~0.2 to ~7–9 g/m^2/h), and measured at 0, 2, and 18 h. Animal experiments were performed at the UIUC animal research facilities at the Urbana-Champaign campus, IL, USA and the subsequent FLIM experiments at the Laboratory for Fluorescence Dynamics, at the time of the experiments located at the Department of Physics, University of Illinois, IL, USA. Preliminary experiments were also performed at UCSF, and control experiments at the Dermatology Department, University Medical Center Hamburg-Eppendorf, and Anatomical Institute, University Hannover, both Germany.

Transmission electron microscopy (TEM)

Biopsies from mouse skin freshly obtained at time points matching the dye application protocol and earlier (untreated, 1,2,18 h) were fixed directly for 48 h in Karnovsky′s fixative [33], washed in PBS, and postfixed in buffered 1% osmium tetroxide [52]. After careful dehydration in graded ethanol, the skin samples were embedded in Epon 812 (Serva) [45] and cut with a diamond knife on an ultramicrotome Ultracut E (Leica). Thin sections (<100 nm) were stained with methanolic uranyl acetate [67] and lead citrate [61], then viewed in an electron microscope EM10C (Zeiss) operated at 60 kV.

Fluorescence microscopy

Calcium Green 5N was applied once (5 ul of a 0.1 mM solution in DMSO, to an approximate area of 5 mm diameter), and a biopsy was taken 18 h following dye application, in preliminary experiments also at 1 and 2 h, mounted for microscopy, and directly visualized. Control images to assess dye distribution in skin were taken on a Zeiss Axiophot, equipped with a Hamamatsu C7472 camera. For this purpose, freshly obtained hairless mouse skin biopsies in OCT compound were flash-frozen in liquid nitrogen, cut on a cryostat to 6 µm sections, coverslipped and viewed.

Experimental procedure

TEM, fluorescence microscopy, pH and TEWL measurements as well as the preliminary work to establish the choice of dye, were conducted as separate experiments. The functional experiments, imaging of calcium distribution via FLIM pre- and post-barrier abrogation were conducted as follows: Calcium Green 5N was applied once to one flank area of an anesthetized mouse. 18 h following dye application, a biopsy was taken without further treatment for one area. Barrier abrogation was performed on separate animals, treated otherwise identically, as the imaging process overall was too lengthy to conserve biopsies from one animal for both conditions.

Fluorescence lifetime imaging microscopy

In brief, two-photon FLIM to determine calcium was performed using a Millenia-pumped Tsunami titanium:sapphire laser system (Spectra-Physics) as the two-photon excitation source. Excitation of the sample was achieved by coupling the 800 nm output of the laser through the epi-fluorescence port of a Zeiss Axiovert microscope. The fluorescence was collected using a Hamamatsu (R3996) photomultiplier placed at the bottom port of the microscope. Scanning mirrors and a 40× infinity corrected oil objective (Zeiss F Fluar, 1.3 N.A.) were used. Z-slices (1.7 µm per slice) were obtained by adjusting the objective focus with a motorized driver (ASI Multi-Scan 4). Lifetime data were acquired using time-correlated single photon counting (TCSPC). Fluorescein was used as the reference lifetime standard (τ_f = 4.05 ns, pH 9.5). Background fluorescence was determined to be negligible, in accordance with our prior data [26]. Additionally, DMSO was not expected to alter our measurements as its use in fluorescence is facilitated because of its optical transparency [87].

Further, background fluorescence would be excluded via phasor analysis (see below). Data evaluation and visualization were performed directly with the in-house software SIM-FCS (http://www.lfd.uci.edu/globals/). Individual images were combined using Adobe Illustrator (Adobe Systems Incorporated, San Jose, CA, USA), but no further image processing was performed. Background fluorescence was measured in samples of unstained tissue, treated otherwise identically. To facilitate comparison of different experimental conditions, i.e., various dyes and skin pretreatments, we imaged morphologically similar sites, where the columnar arrangement in SC also, if to a lesser degree, is reflected in a regular arrangement of cells in layers underneath [12, 30, 82], as outlined in a prior publication [5].

Calibration via phasor plot

Briefly, in time-correlated single photon counting multiple lifetime components from different molecular species or different conformations of the same molecule are analyzed via exponential fitting of decay times, pixel by pixel for lifetime imaging. The phasor approach decomposes the decay into Fourier components for mathematical analysis in vector algebra, which is more easily computed than exponential fitting routines. Different proportions of the two fluorescent species expected for the indicator molecules used, here calcium-bound and free dye, arrange in one line in the geometrical display of such vectors, the phasor plot (Figs. 2, 3, panels e). Artifact components from background or other molecular species will not arrange along that same line, and are thus identified and excluded from the evaluation (for further detail please refer to [16]). Nevertheless, in the experiments presented here, we did not observe such effects. The images presented here were recalculated and are displayed calibrated based on the phasor plot derived from a calibration in a series of calcium-containing buffers (see "Results").

Results

Preliminary experiments

Dye application and distribution, tissue morphology, and epidermal function

In preliminary experiments, we tested dyes from the Calcium Green- and Rhod-series, and settled on CaG5N as its use resulted most advantageous for its quantum yield and range of calcium sensitivity (14 μM, Invitrogen/Molecular Probes), as suggested by a number of prior publications [13, 39, 43, 59, 76]. This dye is only poorly soluble in the recommended pH >6 aqueous medium (Invitrogen/Molecular Probes), or alcoholic solution and did not penetrate epidermis in these solvents. Fluorescence could therefore be detected at the SC surface only (not shown). We next injected CaG1 in DMSO intraepidermally and followed dye distribution/fluorescence over time. Within 30 min, we could observe the regular aspect where epidermal cells could easily be distinguished (data not shown). Nevertheless, the dye injection and the following intraepidermal distribution resulted poorly reproducible. We therefore established topical application of a dye–DMSO solution to the skin of hairless mice as routine for our experiments. Dye distribution across the epidermis following topical application was exemplarily assessed with standard fluorescence microscopy, showing a distribution gradient, but nevertheless dye penetration across the entire epidermal depth (Fig. 1c). We next performed a number of control experiments to assess whether the application of DMSO left a discernible effect on epidermal permeability barrier function. Macroscopically, application of DMSO leads to the known wheal [34] (Fig. 1a), and after its disappearance (at the earliest between 60 and 90 min post application) when a dye–DMSO solution was applied, a slightly stained spot remained (Fig. 1b), which was biopsied at 18 h for lifetime experiments. By electron microscopy (EM) of dye–DMSO-exposed skin, compared to untreated, gross morphology, as well as nuclei/ER/SC appeared normal at all time points (1, 2, 18 h) (Fig 1d, 18 h). At 1 h, occasional vacuoles in granular layer cells could be observed (not shown); further ultrastructural alterations were not detected and therefore we did not routinely perform further EM controls.

In control experiments parallel to dye application, we assessed changes in TEWL and surface pH following DMSO application. Changes in surface pH over time were observed, i.e., an initial rise of about 0.5 pH units over the first 2 h, and restoration to initial values by 18 h. As treated and untreated mice (i.e., mice which had been anesthetized to measure pH and TEWL) displayed identical behavior, we attributed these changes to stress of manipulation [15], side effects of anesthesia, and circadian rhythm [18]. TEWL underwent similar, although transitory larger changes, which were to be expected for the solvent properties of DMSO. Initially, in parallel to the wheal reaction, there was a steep rise of TEWL in DMSO treated skin, which subsided, i.e., returned to within less than 15% difference of starting value, 18 h following DMSO application (data not shown). Further, in initial experiments we compared the Ca^{2+} distribution in biopsies taken at 2 and 18 h following application of CaG5N in DMSO. We did not discern any major differences between these time points, and for reasons of practicability chose the latter, overnight time point thus also excluding lingering DMSO effects. Finally, none of the mice treated in this manner ever

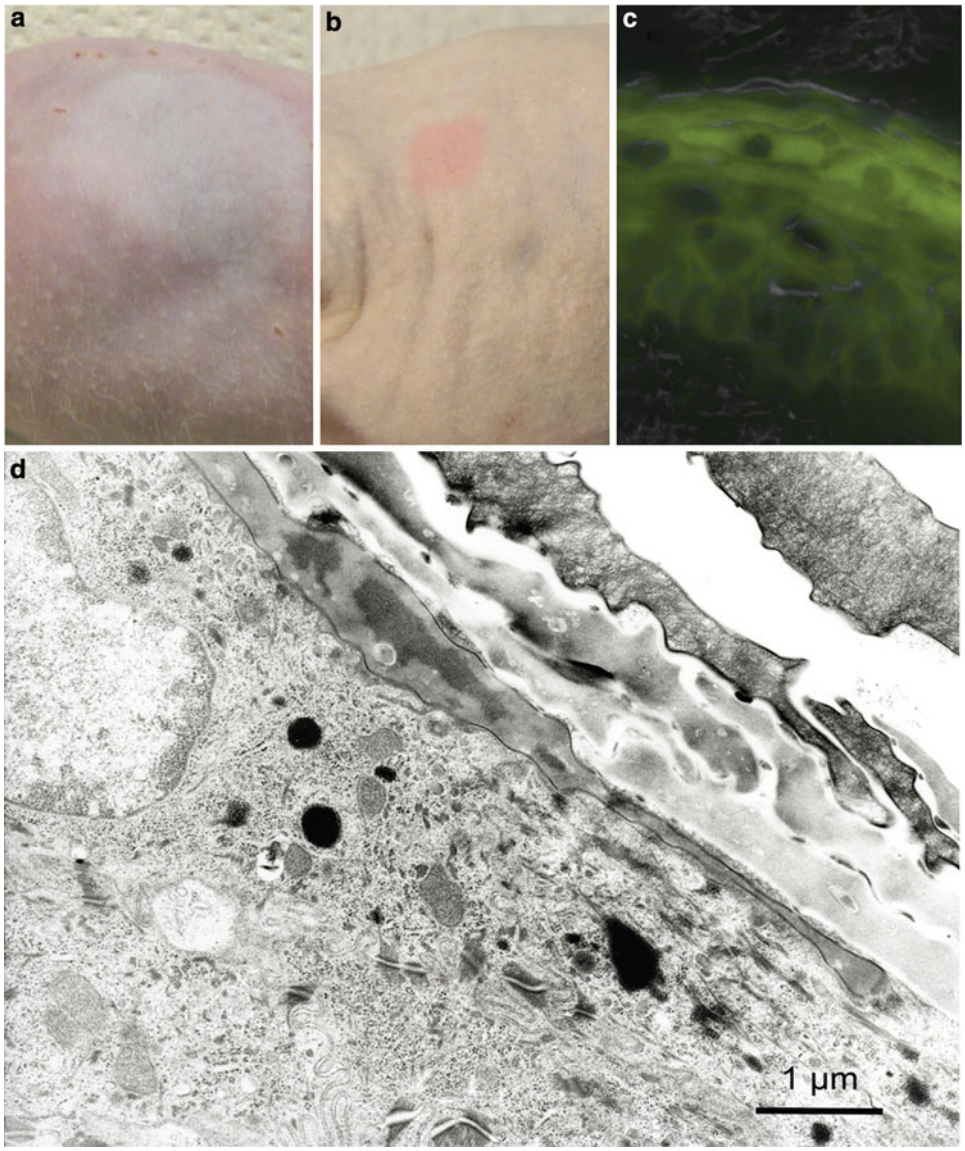

Fig. 1 Topical dye/DMSO application and distribution, and gross and tissue morphology. Panel **a** wheal reaction from DMSO only. Panel **b** CaG5N spot remaining at 18 h post application in DMSO. Panel **c** fluorescence microscopy image of a histologic section of mouse skin, CaG5N distribution 18 h following application in vivo. Panel **d** electron micrograph of mouse skin at 18 h post DMSO application

displayed signs of discomfort, or scratching at the site of dye–DMSO application.

Calibration of CaG5N in lifetime experiments

For in vitro calibration, we used established buffer kits [72], in the highest concentrations on occasion extended with solutions prepared from a calcium chloride stock. We repeatedly performed single-point fluorescence measurements, using different buffer batches to exclude dilution errors. We found very little variation in the buffer measurements (at $n = 4$ an SEM between 0.00 and 0.20), with the resulting K_d of 4.9 μM, well in range with other reported calibrations (see Table 2). Such buffer systems [72] address correction for viscosity [58], ionic strength [27], and presence of proteins [55, 62]. Also, in our prior work on lifetime measurements of pH in SC, we established that lipids, i.e., a saturated solution of cholesterol, did not alter K_d [5]. Nevertheless, for the purposes of this study, measurements in the protein-rich epidermal layers rather than SC, it appeared imperative to ascertain the influence of protein on the calibration. To test whether presence of protein affected K_d, we added BSA in increasing concentrations (9.1–20%) to the buffer system. As the BSA used contained calcium (according to specifications between 0.004 and 0.007%), a shift corresponding to less than 0.005 mM calcium was to be expected. Instead, we found an attenuation of sensitivity, introduced in both the low and high concentration ranges; similar dye behavior has been reported earlier for CaG1 [70]. Yet, most importantly, the resulting K_d underwent only little change (less than 0.6 μM between buffer and highest BSA concentration), and these measurements were as invariant as the buffer-only measurements. Consequently, and for reasons of reproducibility, we based fur-

Table 2 CaG5N calibrations reported

References	Tissue/target	Kd (μM)	Calibration	Comments
Combettes [13]	Rat hepatocyte IP_3	35	In vivo/in vitro	in vivo on hepatocytes; identical values in vitro and in vivo
Eilers [19]	Rat cerebellar Purkinje neurons	17	In vitro	Use of CaG5 N to reduce buffering of Ca^{2+}
Escobar [22]	Frog skeletal muscle fibers	45	In vitro	Calibration via Fmin/Fmax; patch-clamp controlled
Hixon [29]	Recombinant cytosolic PLA2	50	In vitro	
Kubitscheck [38]	Erythrocytes	2	In vivo	Calibration on erythrocyte ghosts
Llano [43]	Rat cerebellar basket cell axons	20	In vitro	Rationale for choice of dye
Naraghi [54]	in vitro only	23.1	In vitro	
Peretz [57]	Drosophila photoreceptors	25	Not mentioned	
Rajdev [59]	Rat brain neurons	4.3	In vivo/in vitro	Additionally in vivo calibration determining Fmin/Fmax
Tucker [75]	Turtle hair cells	25	In vitro	
		32	In vivo	
Ukhanov [76]	Limulus ventral photoreceptor	67	In vitro	Fluorescence ratio measurements using ANTS, Ca^{2+}-sensitive electrode controlled, Mg^{2+} had no effect
Vergara [77]	Skeletal muscle fibers	85	In vitro	
Walz [79]	Honeybee drone photoreceptors	74	In vitro	
Wang [80]	Aging mouse skeletal muscle fibers	31	In vivo	Calibration on muscle fibers
Wang [81]	Adult skeletal muscle fibers	33	In vitro	
Yao [86]	Xenopus oocytes	10–12	In vitro	No effect of CaG5N on oscillatory membrane current responses
Zhao [88]	Frog skeletal muscle fibers			Protein binding of dyes affected response time, not sensitivity; extensive dye comparison
		156	In vivo	Absorbance in muscle fibers
		63	In vitro	Absorbance measurements

An extensive literature search yielded a number of publications where CaG5N was calibrated. The table lists reports with original determinations of K_d values for Ca^{2+} binding, with the tissues investigated, and method of calibration. In vitro calibrations generally were performed using a defined calcium buffer series, as used for the experiments reported in this manuscript, or similar buffer systems. Values in this table were obtained using the method of fractional changes in fluorescence (ΔF) above the resting baseline (ΔF/F)

Given the fact that different methods and setups were used, the wide span of values is not surprising. Our resulting K_d of 4.9 μM fits well into the range of most values (refer to "Results")

ther calculations on the K_d derived from measurements in the prefabricated calcium-buffer kit without protein additions. This process is further validated through the use of the phasor plot, which requires only a K_d to compute images (ref. to "Methods" and [11]).

The phasor plot offers a number of advantages for the purpose of imaging ionic concentrations; our recent paper [11] further details this method beyond the already published concept [16]. In short, this approach displays the whole of calcium-values obtained in the image series presented here (Figs. 2, 3, phasor plots in panels e) in form of a cloud, superimposed with the calibration-curve obtained in buffers of distinct calcium concentrations. The distribution of experimentally obtained values along this calibration graph therefore justifies the choice of dye, as values are evenly spread along and around the calibration plot. Had we chosen an indicator dye with a sensitivity range not suited for our samples, experimental values could be expected to arrange towards the low or high end of the calibration graph, or not be covered by the calibration altogether. Different fluorescent species than the two forms expected from the indicator dye (e.g., from other, interfering ions) would likewise be evident in the phasor plot, but were not observed. In different approaches to lifetime-analysis such species would be difficult to discern, but, when present, complicate mathematical fittings. Further, a shift of pH would only affect the SC-extracellular domain, as shown in our prior data [5, 6, 26]. Thus, we concluded that our measurements were suitable for rodent skin, and artifactual lifetime components were not present in our images.

Calcium distribution in epidermis at steady state

We initially tried to establish whether typical concentration ranges for distinct areas of epidermis existed, in parallel to the reported calcium gradient across epidermis (please also

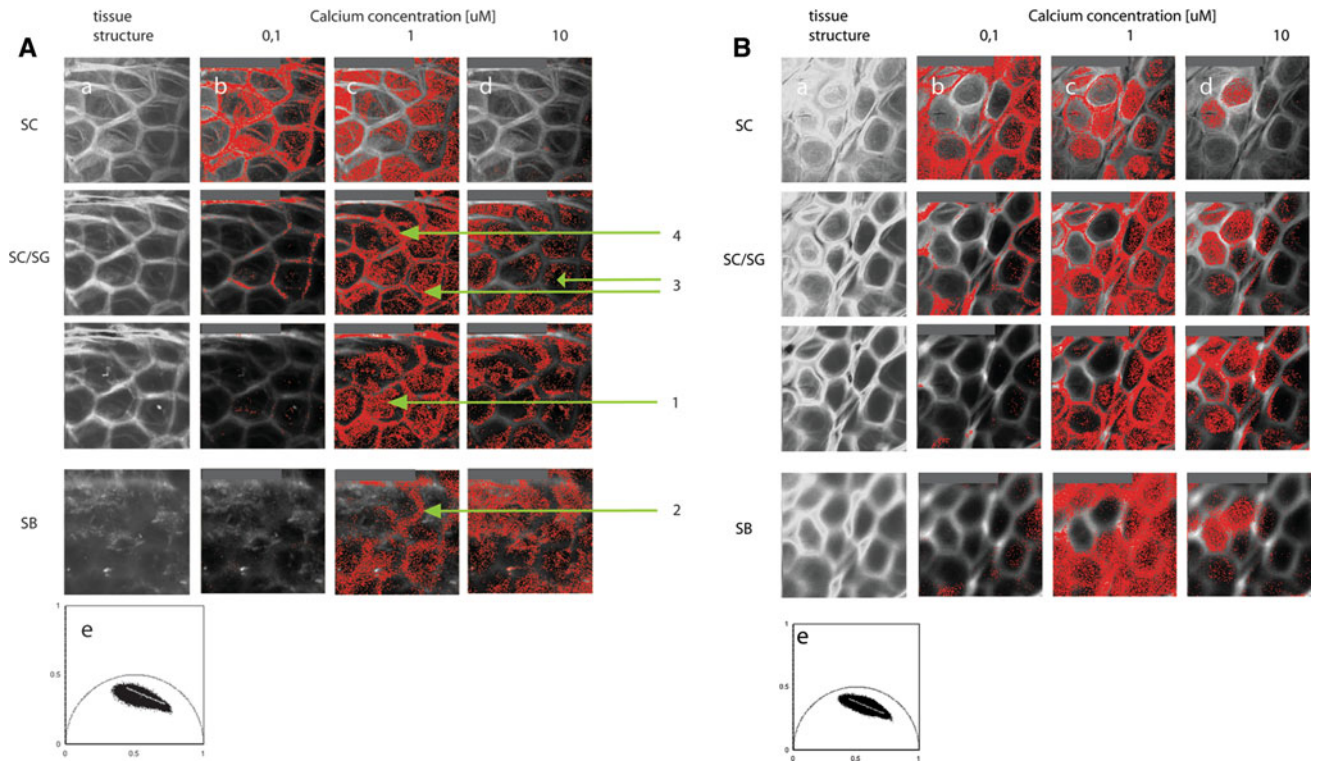

Fig. 2 Calcium distribution and concentrations in undisturbed rodent epidermis, two figures from separate experiments. Fluorescence lifetime imaging of hairless mouse skin, stained with CaG5N overnight to image areas of 107 μm^2. Experiments were performed in triplicate ($n \geq 3$), and typical images are shown here. Column *a*: fluorescence-intensity images were adjusted to enhance structural features and to visualize progression of the microscopic focus in *z*-direction into the epidermis. SC to SG and following are continuous images, two further optical sections until reaching the SB were omitted Columns *b–d*: images identical to column *a*, overlaid with the *red* signal indicating calcium distribution at the concentrations indicated at the top of the columns. Panel *e*: phasor plot of the cloud of calcium values in the universal phasor circle. The cloud represents all values of the panels in columns *b–d*, overlaid with the calibration line resulting from the series of calcium-containing buffers used to calculate the calcium signal in columns *b–d*. *Arrows* to indicate specific concentrations, in Fig. 2**a**, please also refer to "Results": intracellular compartments (*arrow 1*). Extracellular compartment in lower epidermal layers (*arrow 2*). Mutually exclusive subcellular compartments for medium and high concentrations (*arrows 3*). Intracellular-submembrane accumulation for the intermediate concentration (*arrow 4*)

compare to Table 1). We rather found that within certain value-ranges Ca^{2+} distribution stayed identical. Therefore, the individual images displayed in Figs. 2a, b, 3a, b were set to a low, intermediate and high range (corresponding to columns b, c, and d), at the same time exploiting the sensitivity range of the indicator dye, and in the process resulting to be typical for the extracellular, intracellular, and possibly the bound or calcium-store compartments.

We then used this protocol to ascertain calcium distribution in undisturbed rodent skin, baseline condition for our comparisons. We found low Ca^{2+} concentrations in the extracellular compartment at the surface, i.e., in the interstitial areas of the SC, extending to, but not beyond the SC/SG interface (Fig. 2, first and second rows, column b).

Ca^{2+} concentrations in a medium range can be found throughout the epidermis, restricted to the intracellular compartment of the SC, quasi delineating the cell membranes and intracellular compartment in the SG, with occasional areas of increased Ca^{2+} concentration indicating intracellular compartments (arrow 1), and possibly extending to the extracellular compartment in lower epidermal layers (Fig. 2, first through fourth rows, column c, arrow 2).

High Ca^{2+} concentrations were not found within the SC, but throughout the epidermis and limited to the intracellular compartment only (Fig. 2, second through fourth rows, column d).

As the method and dye application protocol does not allow counterstaining, the only approach to attributing distinct Ca^{2+} concentrations to cellular layers and structures is the comparison of the specific, calibrated calcium signal to the separately displayed fluorescence-intensity images (Figs. 2, 3, columns a), and their progression with the microscopic depth focus. It was therefore impossible to identify specific structures beyond cellular outlines over depth; nevertheless, the outlines generated through the Ca^{2+} signal occasionally appear as mutually exclusive subcellular compartments for medium and high concentrations (e.g., Fig. 2, second row, columns c and d, arrows 3). The mem-

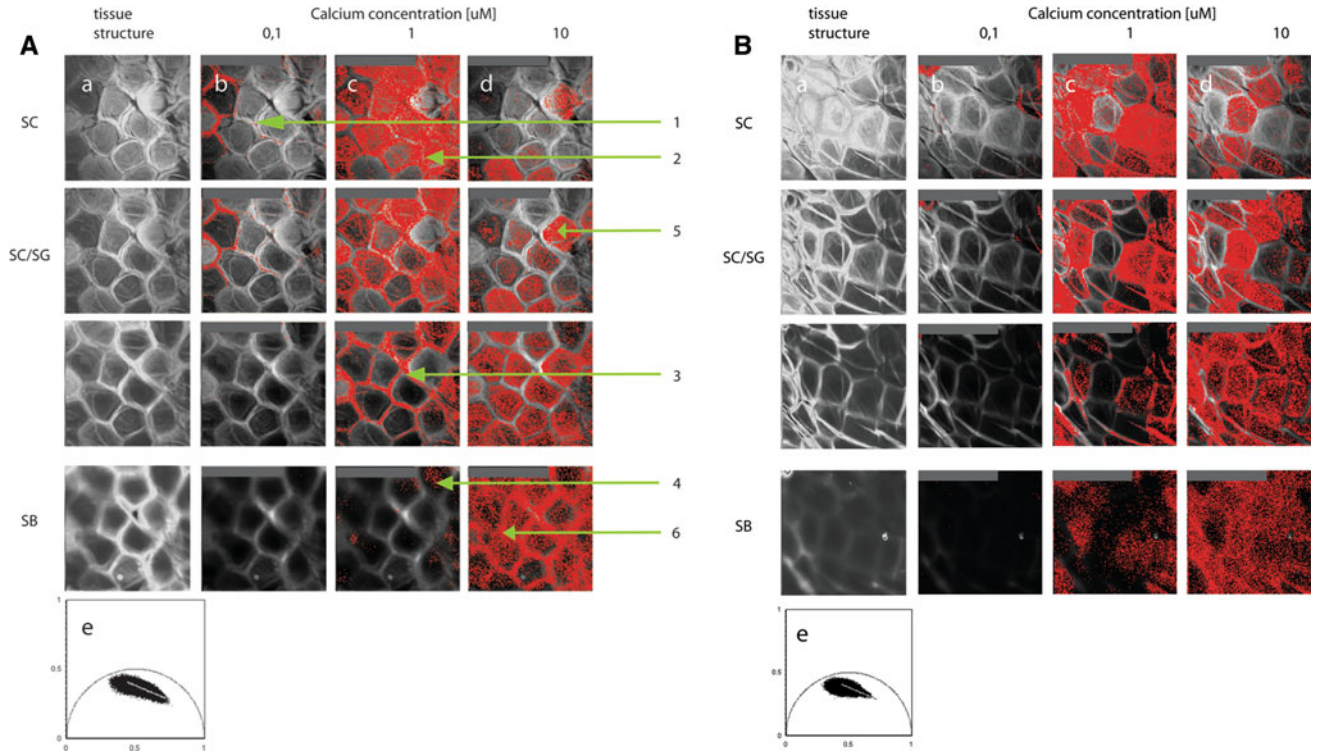

Fig. 3 Calcium distribution and concentrations in barrier-abrogated epidermis, two figures from separate experiments. Samples were taken form separate animals than the undisturbed, treated otherwise identically. Conditions and order of panels matching Fig. 2. Note that the cloud of calcium-values in panel *e* is left-shifted, representing slightly higher values overall. *Arrows* to indicate specific concentrations, in Fig. 3**a**, please also refer to "Results": low Ca^{2+} concentrations extracellularly at the surface and SC/SG interface (*arrow 1*). Medium concentrations intracellulary (*arrow 2*), cell membranes and extracellular compartment (*arrow 3*), and in the stratum basale (*SB*) in intracellular areas (*arrow 4*). High Ca^{2+} concentrations delineating the intracellular compartment in the SG (*arrow 5*) and delineating the cell membranes and cell periphery in the SB (*arrow 6*)

brane delineation via the Ca^{2+} signal may indicate an intracellular-submembrane accumulation for the intermediate concentration, consistent with a signaling role for this concentration range (Fig. 2, column c, second and third rows, arrow 4). Additionally, although an unequivocal in- or exclusion cannot be made at the current resolution, the images are also suggestive of distinct Ca^{2+} concentrations within the extracellular spaces in epidermis. Taken together, we find a specific pattern of Ca^{2+} concentrations at baseline, also summarized in Fig. 4.

Calcium distribution in epidermis following barrier disruption

Finally, we tested this imaging approach on the known, inducible perturbation of Ca^{2+} homeostasis, epidermal permeability barrier abrogation in rodent skin.

The limitations of earlier approaches to calcium imaging were outlined in the introduction, and from a biologic perspective, the time delay between a given physiologic state and its microscopic observation is the largest artifact introduced with an experiment, especially as fast intra- and extracellular calcium signaling is firmly established from cell-culture experiments. We therefore aimed at an early time point for our experiments, and reproducibly could start acquiring images 30 min past tapestrip and preparation of a biopsy for microscopy.

At this early time point, we found low Ca^{2+} concentrations only extracellularly at the surface and SC/SG interface (Fig. 3, first and second rows, column b, arrow 1).

Medium concentrations were found, now more pronounced, intracellulary in the SC to SC/SG interface (arrow 2), while below the SC/SG-interface medium concentrations are shifted to or outline the cell membranes and extracellular compartment of the epidermis (arrow 3), and in the stratum basale (SB) are confined again to intracellular areas (Fig. 3, first through fourth rows, column c, arrow 4).

High Ca^{2+} concentrations post-tapestrip can now be found more evenly distributed throughout the cells in all upper layers (Fig. 3, first through third row, column d), occasionally even intracellularly in the SC (Fig. 3, first row, column d) and increasingly downwards to the SB, at the same time shifting from strictly limited and delineating the intracellular compartment in the SG (arrow 5) to delineating the cell membranes and cell periphery in the SB (Fig. 3, first through fourth rows, column d, arrow 6). Together, we

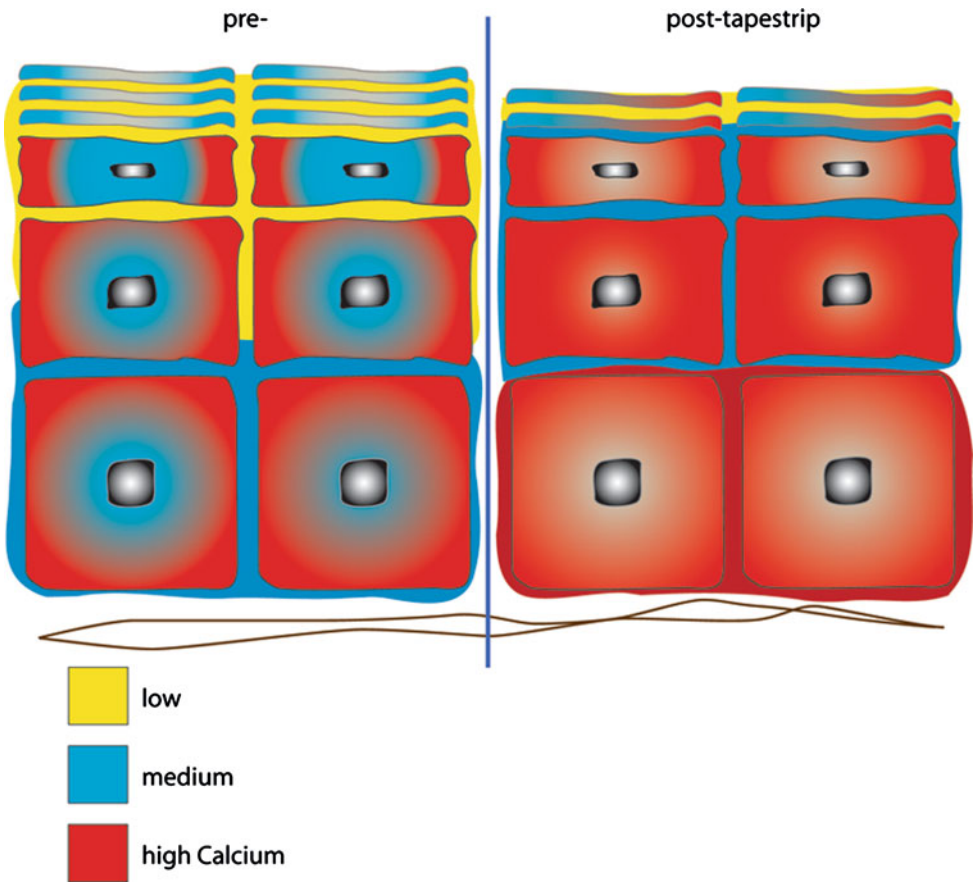

Fig. 4 Schematic summary of results. View of epidermis pre- (*left panel*) and post-tapestrip (*right panel*), summarizing the details of changes in calcium distribution induced by acute barrier disruption. Note the increase in concentrations, from intracellular stores to the cell periphery and extracellular space, then upward in epidermis. The concentration ranges used match the actual data displayed in Figs. 2, 3, i.e., *low* (0.1 μM), *medium* (1 μM), and *high* (10 μM)

find a rapid shift of Ca^{2+} towards higher concentrations and apical epidermal layers, including SC. As a summary of our findings please refer to Fig. 4.

Discussion

Technical considerations and limitations

The comparison to calcium values reported elsewhere or obtained from different experiments fits well with our findings (refer to Tables 1, 2), with several technical caveats:

First, we could not detect calcium below the epidermis, which we attribute to the anatomy of rodent skin where very little dermal structure and therefore no label acquiring, i.e., calcium-binding or -retaining structures could be observed. In other species, the dermal compartment might serve as an internal reference, as values from serum should equal concentrations found in dermis (see legend to Table 1). Thus, in rodent skin only basal-layer values may be compared to serum levels. In our data, the intermediate range values to be found intra- and extracellularly in the basal layer of non-disrupted skin appears as the next best reference, and again fits with these findings.

Second, of concern are also the physico-chemical characteristics of DMSO; it is a hygroscopic, amphiphilic, aprotic, small size solvent for organic and inorganic compounds as well as macromolecules [87], which readily penetrates biological membranes and skin. There is a large body of work on the use of DMSO as a cryoprotectant, and since the initial description and speculation on possible mechanisms [44], there was little progress in elucidating the mechanisms involved. A recent and detailed review on the use of DMSO [64] lists multiple pharmacological, cellular, and molecular aspects. Transient, rather rapid effects on calcium, observed in cells and isolated organs also were reported. From our preliminary experiments to establish the method used here, we concluded that the 18-h delay between application of DMSO and the functional experiments had a compensatory effect, leading to complete absorption of the minor amount from skin and elimination from the living animal. Accordingly, our control experiments demonstrated only an early and transiently affected epidermal function and no further discernible untoward effects of DMSO. As corroborating observation might serve the fact that we did not find an accumulation of CaG5N fluorescence inside corneocytes in undisturbed epidermis (Fig. 1, panel c), where the most direct or intense DMSO

exposition occurred. Also, the distinct FLIM signal from this compartment is in accordance with the underlying layers (compare first and second rows, Figs. 2, 3). Based on these reports and our preliminary experiments to establish CaG5N labeling, we considered the use of DMSO safe and non-interfering in our experimental protocol.

Third, in respect to the indicator dye, there is the additional, general caveat that there may be more-than-single-site Ca^{2+} binding at low Ca^{2+} concentration [76, 88]. A different, to date unpublished explanation of this effect postulates two fluorescent species at low-to-zero Ca^{2+}, where free Calcium green-1 has a closed form with short lifetime, and an open, bound to Ca^{2+} form with longer lifetime (personal communication; David Jameson, University of Hawaii). For its chemical structure, this concern should apply to CaG5N also, but is also resolved through the phasor analysis, which eliminates a host of artifacts common to fluorescence based methods (see Preliminary Experiments).

Lastly, we here present data early following barrier disruption, as such observations were heretofore not possible. A series of experiments covering the complete time-course of epidermal permeability barrier recovery will hopefully provide more insight. At the same time, our prior work described the changes of pH within the extracellular compartment of the SC [5] in response to barrier disruption, which we now show similarly for calcium within epidermis. Whether and how both calcium and pH are mechanistically connected is unclear, but such a connection might follow also from our prior work [3, 20, 21]; both aspects are topic of an ongoing project in our lab.

Findings in skin

As compared to earlier reports on Ca^{2+} in skin, our images display Ca^{2+} distribution and their dynamics in epidermis in detail in close to in vivo conditions. Intra- and extracellular compartments across epidermal depth can mostly be distinguished, and although subcellular compartments cannot be identified in our approach, a number of images hint at intracellular structures, and at least suggest the existence of intracellular stores of higher Ca^{2+} concentration, which are firmly established through other methods [51].

Through previous observations only a uniform calcium gradient across epidermal depth could be distinguished (see "Introduction"), and the redistribution upon barrier abrogation was known, although with limited detail. The experimental data shown here depict the dynamic, cellular redistribution of calcium in epidermis following a barrier insult, as summarized in Fig. 4 and thus partially contradicts the previous concept. In undisturbed skin, low concentrations are found from surface to SC/SG interface, and medium concentrations below these layers. Upon barrier disruption, we found a fast change of Ca^{2+} distribution. The lowest concentrations almost disappear, while medium and higher concentrations are now present in SG and SB, respectively. The pattern emerging from this more detailed view now shows a shift of calcium upon barrier insult, from deeper-layer compartments, moved to the cell membranes and upward through the epidermis, a dynamic shift within cellular localizations and epidermal layers. This same shift, although at the resolution of our images not entirely distinguishable, can be found in the extracellular spaces. Overall, calcium is shown in a differential distribution, which still may be viewed as a gradient of sorts, albeit barrier disruption, with the time-wise closer look provided in the method described here, shows no abrogation of the Ca^{2+} gradient. Our findings are summarized schematically in Fig. 4. The membrane orientation of calcium upon barrier insult is consistent with a signaling role of calcium. The upward shift of higher concentrations following barrier disruption indicates a calcium-loss when barrier function is defective, but also its involvement in the biochemistry of barrier repair. Probably temporarily, these shifts involve an extracellular rise in calcium, for the upward shift and eventual loss in case of a defective barrier. Furthermore, a rapid barrier restoration may even hint at a calcium-conserving strategy, which is mostly known from bone metabolism and the interplay of vitamin D and parathyroid hormone to maintain calcium-levels (e.g., [66]). In epidermis, especially in the case of psoriasis this also holds true, although further roles and functions remain to be explored (e.g., [60]).

With FLIM, we now visualize close to in vivo biologically relevant changes of Ca^{2+} distribution over epidermal depth, at cellular resolution, without tissue processing, minimizing artifact. Specifically, TCSPC offers precision at low light intensities, and in conjunction with the novel phasor analysis, visual control over the exclusion of artifactual contributions in the mathematical analysis is provided. We view this approach as key to further insight into regulation, coordination and orchestration of barrier repair and other calcium-dependent processes in skin. Future experiments, using advanced equipment currently being established, will allow us to gain further insight into the time-dependent processes of reestablishing barrier function, and will have to show whether it is barrier status per se which regulates the formation of the epidermal calcium gradient, as earlier data shows [20], or if calcium itself contributes to the regulation of barrier status.

Finally, with increasing dissemination of two-photon-equipment, the method used here should become more frequently utilized and help to extend this approach beyond rodent epidermis into deeper layers of mammal epidermis at subcellular resolution.

Acknowledgments This work was supported through a grant from the European Community's Marie-Curie-Program, MC-IRG 6675 (to

MB). We thank Mrs. Monika Thiel for expert assistance in preparing graphics

Conflict of interest The authors declare that they have no conflict of interest.

References

1. Agronskaia AV, Tertoolen L, Gerritsen HC (2004) Fast fluorescence lifetime imaging of calcium in living cells. J Biomed Opt 9:1230–1237
2. Aronchik I, Behne MJ, Leypoldt L, Crumrine D, Epstein E, Ikeda S, Mizoguchi M, Bench G, Pozzan T, Mauro T (2003) Actin reorganization is abnormal and cellular ATP is decreased in Hailey–Hailey keratinocytes. J Invest Dermatol 121:681–687
3. Behne MJ, Barry NP, Hanson KM, Aronchik I, Clegg RW, Gratton E, Feingold K, Holleran WM, Elias PM, Mauro TM (2003) Neonatal development of the stratum corneum pH gradient: localization and mechanisms leading to emergence of optimal barrier function. J Invest Dermatol 120:998–1006
4. Behne MJ, Tu CL, Aronchik I, Epstein E, Bench G, Bikle DD, Pozzan T, Mauro TM (2003) Human keratinocyte ATP2C1 localizes to the Golgi and controls Golgi Ca^{2+} stores. J Invest Dermatol 121:688–694
5. Behne MJ, Meyer JW, Hanson KM, Barry NP, Murata S, Crumrine D, Clegg RW, Gratton E, Holleran WM, Elias PM, Mauro TM (2002) NHE1 regulates the stratum corneum permeability barrier homeostasis. Microenvironment acidification assessed with fluorescence lifetime imaging. J Biol Chem 277:47399–47406
6. Behne MJ, Barry NP, Moll I, Gratton E, Mauro TM (2004) Fluorescence lifetime to image epidermal ionic concentrations. In: Avrillier S, Tualle JM (eds) Femtosecond laser Applications in Biology. Proceedings of SPIE, Bellingham, WA, pp 37–44
7. Bikle DD, Ratnam A, Mauro T, Harris J, Pillai S (1996) Changes in calcium responsiveness and handling during keratinocyte differentiation. Potential role of the calcium receptor. J Clin Invest 97:1085–1093
8. Brini M, Carafoli E (2000) Calcium signalling: a historical account, recent developments and future perspectives. Cell Mol Life Sci 57:354–370
9. Bunse T, Steigleder GK, Hofert M, Gonsior B (1991) PIXE analysis in uninvolved skin of atopic patients and aged skin. Acta Derm Venereol 71:287–290
10. Celli A, Mackenzie DS, Crumrine DS, Tu CL, Hupe M, Bikle DD, Elias PM, Mauro TM (2010) Endoplasmic reticulum Ca^{2+} depletion activates XBP1 and controls terminal differentiation in keratinocytes and epidermis. Br J Dermatol
11. Celli A, Sanchez S, Behne M, Hazlett T, Gratton E, Mauro T (2010) The epidermal $Ca(^{2+})$ gradient: measurement using the phasor representation of fluorescent lifetime imaging. Biophys J 98:911–921
12. Christophers E (1971) Cellular architecture of the stratum corneum. J Invest Dermatol 56:165–169
13. Combettes L, Cheek TR, Taylor CW (1996) Regulation of inositol trisphosphate receptors by luminal Ca^{2+} contributes to quantal Ca^{2+} mobilization. EMBO J 15:2086–2093
14. Davies EV, Hallett MB (1998) High micromolar Ca^{2+} beneath the plasma membrane in stimulated neutrophils. Biochem Biophys Res Commun 248:679–683
15. Denda M, Tsuchiya T, Elias PM, Feingold KR (2000) Stress alters cutaneous permeability barrier homeostasis. Am J Physiol Regul Integr Comp Physiol 278:R367–R372
16. Digman MA, Caiolfa VR, Zamai M, Gratton E (2008) The phasor approach to fluorescence lifetime imaging analysis. Biophys J 94:L14–L16
17. Dupont G, Combettes L, Leybaert L (2007) Calcium dynamics: spatio-temporal organization from the subcellular to the organ level. Int Rev Cytol 261:193–245
18. Ehlers C, Ivens UI, Moller ML, Senderovitz T, Serup J (2001) Comparison of two pH meters used for skin surface pH measurement: the pH meter 'pH900' from Courage & Khazaka versus the pH meter '1140' from Mettler Toledo. Skin Res Technol 7:84–89
19. Eilers J, Callewaert G, Armstrong C, Konnerth A (1995) Calcium signaling in a narrow somatic submembrane shell during synaptic activity in cerebellar Purkinje neurons. Proc Natl Acad Sci USA 92:10272–10276
20. Elias P, Ahn S, Brown B, Crumrine D, Feingold KR (2002) Origin of the epidermal calcium gradient: regulation by barrier status and role of active vs passive mechanisms. J Invest Dermatol 119:1269–1274
21. Elias PM, Nau P, Hanley K, Cullander C, Crumrine D, Bench G, Sideras-Haddad E, Mauro T, Williams ML, Feingold KR (1998) Formation of the epidermal calcium gradient coincides with key milestones of barrier ontogenesis in the rodent. J Invest Dermatol 110:399–404
22. Escobar AL, Monck JR, Fernandez JM, Vergara JL (1994) Localization of the site of Ca^{2+} release at the level of a single sarcomere in skeletal muscle fibres. Nature 367:739–741
23. Fan GY, Fujisaki H, Miyawaki A, Tsay RK, Tsien RY, Ellisman MH (1999) Video-rate scanning two-photon excitation fluorescence microscopy and ratio imaging with cameleons. Biophys J 76:2412–2420
24. Forslind B, Werner-Linde Y, Lindberg M, Pallon J (1999) Elemental analysis mirrors epidermal differentiation. Acta Derm Venereol 79:12–17
25. Grundin TG, Roomans GM, Forslind B, Lindberg M, Werner Y (1985) X-ray microanalysis of psoriatic skin. J Invest Dermatol 85:378–380
26. Hanson KM, Behne MJ, Barry NP, Mauro TM, Gratton E, Clegg RM (2002) Two-photon fluorescence lifetime imaging of the skin stratum corneum pH gradient. Biophys J 83:1682–1690
27. Harrison SM, Bers DM (1987) The effect of temperature and ionic strength on the apparent Ca-affinity of EGTA and the analogous Ca-chelators BAPTA and dibromo-BAPTA. Biochim Biophys Acta 925:133–143
28. Hennings H, Holbrook KA, Yuspa SH (1983) Factors influencing calcium-induced terminal differentiation in cultured mouse epidermal cells. J Cell Physiol 116:265–281
29. Hixon MS, Ball A, Gelb MH (1998) Calcium-dependent and -independent interfacial binding and catalysis of cytosolic group IV phospholipase A2. Biochemistry 37:8516–8526
30. Huzaira M, Rius F, Rajadhyaksha M, Anderson RR, Gonzalez S (2001) Topographic variations in normal skin, as viewed by in vivo reflectance confocal microscopy. J Invest Dermatol 116:846–852
31. Hyvonen-Dabek M, Nikkinen-Vilkki P, Dabek JT (1984) Selenium and other elements in human maternal and umbilical serum, as determined simultaneously by proton-induced X-ray emission. Clin Chem 30:529–533
32. Jamora C, Fuchs E (2002) Intercellular adhesion, signalling and the cytoskeleton. Nat Cell Biol 4:E101–E108
33. Karnovsky MJ (1965) A formaldehyde–glutaraldehyde fixative of high osmolality for use in electron microscopy. J Cell Biol 27:137A–138A
34. Kligman AM (1965) Topical Pharmacology and Toxicology of Dimethyl Sulfoxide. 1. Jama 193:796–804
35. Koester HJ, Baur D, Uhl R, Hell SW (1999) Ca^{2+} fluorescence imaging with pico- and femtosecond two-photon excitation: signal and photodamage. Biophys J 77:2226–2236
36. Kostov Y, Harms P, Rao G (2001) Ratiometric sensing using dual-frequency lifetime discrimination. Anal Biochem 297:105–108

37. Kuba K, Nakayama S (1998) Two-photon laser-scanning microscopy: tests of objective lenses and Ca^{2+} probes. Neurosci Res 32:281–294
38. Kubitscheck U, Pratsch L, Passow H, Peters R (1995) Calcium pump kinetics determined in single erythrocyte ghosts by microphotolysis and confocal imaging. Biophys J 69:30–41
39. Kuhn MA (1993) 1,2-Bis(2-Aminophenoxy)Ethane-N,N,N′,N′,-Tetraacetic Acid Conjugates Used to Measure Intracellular Ca^{2+} Concentration. In: Czarnik AW (ed) Fluorescent chemosensors for ion and molecular recognition, American Chemical Society, pp 147–161
40. Kurebayashi N, Harkins AB, Baylor SM (1993) Use of fura red as an intracellular calcium indicator in frog skeletal muscle fibers. Biophys J 64:1934–1960
41. Lee SK, Lee JY, Lee MY, Chung SM, Chung JH (1999) Advantages of calcium green-1 over other fluorescent dyes in measuring cytosolic calcium in platelets. Anal Biochem 273:186–191
42. Li L, Tucker RW, Hennings H, Yuspa SH (1995) Chelation of intracellular Ca^{2+} inhibits murine keratinocyte differentiation in vitro. J Cell Physiol 163:105–114
43. Llano I, Tan YP, Caputo C (1997) Spatial heterogeneity of intracellular Ca^{2+} signals in axons of basket cells from rat cerebellar slices. J Physiol 502(Pt 3):509–519
44. Lovelock JE, Bishop MW (1959) Prevention of freezing damage to living cells by dimethyl sulphoxide. Nature 183:1394–1395
45. Luft JH (1961) Improvements in epoxy resin embedding methods. J Biophys Biochem Cytol 9:409–414
46. Mao-Qiang M, Mauro T, Bench G, Warren R, Elias PM, Feingold KR (1997) Calcium and potassium inhibit barrier recovery after disruption, independent of the type of insult in hairless mice. Exp Dermatol 6:36–40
47. Mauro T, Bench G, Sidderas-Haddad E, Feingold K, Elias P, Cullander C (1998) Acute barrier perturbation abolishes the Ca^{2+} and K^{+} gradients in murine epidermis: quantitative measurement using PIXE. J Invest Dermatol 111:1198–1201
48. Menon GK, Elias PM, Lee SH, Feingold KR (1992) Localization of calcium in murine epidermis following disruption and repair of the permeability barrier. Cell Tissue Res 270:503–512
49. Menon GK, Elias PM (1991) Ultrastructural localization of calcium in psoriatic and normal human epidermis. Arch Dermatol 127:57–63
50. Menon GK, Grayson S, Elias PM (1985) Ionic calcium reservoirs in mammalian epidermis: ultrastructural localization by ion-capture cytochemistry. J Invest Dermatol 84:508–512
51. Michelangeli F, Ogunbayo OA, Wootton LL (2005) A plethora of interacting organellar Ca^{2+} stores. Curr Opin Cell Biol 17:135–140
52. Millonig G (1961) A modified procedure for lead staining of thin sections. J Biophys Biochem Cytol 11:736–739
53. Missiaen L, Robberecht W, van den Bosch L, Callewaert G, Parys JB, Wuytack F, Raeymaekers L, Nilius B, Eggermont J, De Smedt H (2000) Abnormal intracellular ca($^{2+}$) homeostasis and disease. Cell Calcium 28:1–21
54. Naraghi M (1997) T-jump study of calcium binding kinetics of calcium chelators. Cell Calcium 22:255–268
55. Oheim M, Naraghi M, Muller TH, Neher E (1998) Two dye two wavelength excitation calcium imaging: results from bovine adrenal chromaffin cells. Cell Calcium 24:71–84
56. Parekh AB (2003) Store-operated Ca^{2+} entry: dynamic interplay between endoplasmic reticulum, mitochondria and plasma membrane. J Physiol 547:333–348
57. Peretz A, Suss-Toby E, Rom-Glas A, Arnon A, Payne R, Minke B (1994) The light response of Drosophila photoreceptors is accompanied by an increase in cellular calcium: effects of specific mutations. Neuron 12:1257–1267
58. Poenie M (1990) Alteration of intracellular Fura-2 fluorescence by viscosity: a simple correction. Cell Calcium 11:85–91
59. Rajdev S, Reynolds IJ (1993) Calcium green-5N, a novel fluorescent probe for monitoring high intracellular free Ca^{2+} concentrations associated with glutamate excitotoxicity in cultured rat brain neurons. Neurosci Lett 162:149–152
60. Reichrath J (2007) Vitamin D and the skin: an ancient friend, revisited. Exp Dermatol 16:618–625
61. Reynolds ES (1963) The use of lead citrate at high pH as an electron-opaque stain in electron microscopy. J Cell Biol 17:208–212
62. Roe MW, Lemasters JJ, Herman B (1990) Assessment of Fura-2 for measurements of cytosolic free calcium. Cell Calcium 11:63–73
63. Rudolf R, Mongillo M, Rizzuto R, Pozzan T (2003) Looking forward to seeing calcium. Nat Rev Mol Cell Biol 4:579–586
64. Santos NC, Figueira-Coelho J, Martins-Silva J, Saldanha C (2003) Multidisciplinary utilization of dimethyl sulfoxide: pharmacological, cellular, and molecular aspects. Biochem Pharmacol 65:1035–1041
65. Segre J (2003) Complex redundancy to build a simple epidermal permeability barrier. Curr Opin Cell Biol 15:776–782
66. Staud R (2005) Vitamin D: more than just affecting calcium and bone. Curr Rheumatol Rep 7:356–364
67. Stempak JG, Ward RT (1964) An improved staining method for electron microscopy. J Cell Biol 22:697–701
68. Stout AK, Reynolds IJ (1999) High-affinity calcium indicators underestimate increases in intracellular calcium concentrations associated with excitotoxic glutamate stimulations. Neuroscience 89:91–100
69. Szmacinski H, Lakowicz JR (1995) Possibility of simultaneously measuring low and high calcium concentrations using Fura-2 and lifetime-based sensing. Cell Calcium 18:64–75
70. Thomas D, Tovey SC, Collins TJ, Bootman MD, Berridge MJ, Lipp P (2000) A comparison of fluorescent Ca^{2+} indicator properties and their use in measuring elementary and global Ca^{2+} signals. Cell Calcium 28:213–223
71. Tordoff MG, Bachmanov AA, Reed DR (2007) Forty mouse strain survey of water and sodium intake. Physiol Behav 91:620–631
72. Tsien R, Pozzan T (1989) Measurement of cytosolic free Ca^{2+} with quin2. Methods Enzymol 172:230–262
73. Tu CL, Oda Y, Komuves L, Bikle DD (2004) The role of the calcium-sensing receptor in epidermal differentiation. Cell Calcium 35:265–273
74. Tu CL, Chang W, Bikle DD (2007) The role of the calcium sensing receptor in regulating intracellular calcium handling in human epidermal keratinocytes. J Invest Dermatol 127:1074–1083
75. Tucker T, Fettiplace R (1995) Confocal imaging of calcium microdomains and calcium extrusion in turtle hair cells. Neuron 15:1323–1335
76. Ukhanov KY, Flores TM, Hsiao HS, Mohapatra P, Pitts CH, Payne R (1995) Measurement of cytosolic Ca^{2+} concentration in Limulus ventral photoreceptors using fluorescent dyes. J Gen Physiol 105:95–116
77. Vergara J, Escobar A (1993) Detection of Ca^{2+} transients in skeletal muscle fibers using the low affinity dye Calcium-Green-5N. Biophys J 64:A37
78. Vicanova J, Boelsma E, Mommaas AM, Kempenaar JA, Forslind B, Pallon J, Egelrud T, Koerten HK, Ponec M (1998) Normalization of epidermal calcium distribution profile in reconstructed human epidermis is related to improvement of terminal differentiation and stratum corneum barrier formation. J Invest Dermatol 111:97–106
79. Walz B, Zimmermann B, Seidl S (1994) Intracellular Ca $^{2+}$ concentration and latency of light-induced Ca $^{2+}$ changes in photoreceptors of the honeybee drone. J Comp Physiol [A] 174:421–431
80. Wang ZM, Messi ML, Delbono O (2000) L-Type Ca($^{2+}$) channel charge movement and intracellular Ca($^{2+}$) in skeletal muscle fibers from aging mice. Biophys J 78:1947–1954

81. Wang ZM, Messi ML, Delbono O (1999) Patch-clamp recording of charge movement, Ca($^{2+}$) current, and Ca($^{2+}$) transients in adult skeletal muscle fibers. Biophys J 77:2709–2716
82. Wepf R, Richter T, Koenig K, Dunckelmann K, Sattler M, Biel S, Hintze U, Wittern KP (2002) Re-viewing the structure of the stratum corneum: corneocytes embraces each other. J Invest Dermatol (Abstr 256) 119:250
83. White C, McGeown G (2002) Imaging of changes in sarcoplasmic reticulum [Ca($^{2+}$)] using Oregon Green BAPTA 5N and confocal laser scanning microscopy. Cell Calcium 31:151–159
84. Wieland P, Fischer JA, Trechsel U, Roth HR, Vetter K, Schneider H, Huch A (1980) Perinatal parathyroid hormone, vitamin D metabolites, and calcitonin in man. Am J Physiol 239:E385–E390
85. Wilms CD, Schmidt H, Eilers J (2006) Quantitative two-photon Ca^{2+} imaging via fluorescence lifetime analysis. Cell Calcium 40:73–79
86. Yao Y, Parker I (1994) Ca^{2+} influx modulation of temporal and spatial patterns of inositol trisphosphate-mediated Ca^{2+} liberation in Xenopus oocytes. J Physiol 476:17–28
87. Yu ZW, Quinn PJ (1994) Dimethyl sulphoxide: a review of its applications in cell biology. Biosci Rep 14:259–281
88. Zhao M, Hollingworth S, Baylor SM (1996) Properties of tri- and tetracarboxylate Ca^{2+} indicators in frog skeletal muscle fibers. Biophys J 70:896–916